Available online at www.worldnewsnaturalsciences.com

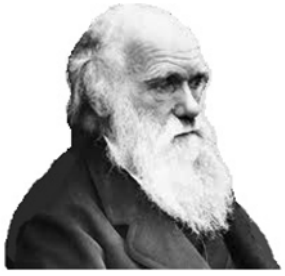

World News of Natural Sciences

WNOFNS 13 (2017) 10-26 EISSN 2543-5426

Batch Removal of Metanil Yellow (MY) from Aqueous Solution by Adsorption on HNO_3-Treated-H_3PO_4-Activated Carbon (NATPAAC) from *Gmelina aborea (G. aborea)* Bark: Kinetic and Mechanism Studies

B. O. Isiuku*

Department of Chemistry, Imo State University, PMB 2000, Owerri, Nigeria

E-mail address: obinnabisiuku@yahoo.com

*Corresponding author: Tel. +2348035731300

M. O. Onyema

Department of Pure and Industrial Chemistry, University of Port Harcourt, PMB 5323, Choba, Port Harcourt, Nigeria

E-mail address: onyemark@yahoo.com

ABSTRACT

Metanil Yellow dye was removed from aqueous solution by batch adsorption on NATPAAC from *G. aborea* bark. Effects of initial dye concentration (C_o), initial pH and adsorbent dosage at 29 °C were studied. Experimental equilibrium adsorption capacities (q_e) obtained, were 2.35, 1.00 and 0.48 mg/g for C_o 25, 50 and 100 mg/L respectively. The kinetics and mechanism of the adsorption were modeled by fitting experimental data into the pseudo-second order (PSO), Elovich, intra-particle diffusion, liquid film diffusion and Boyd models. Results show that the PSO and Elovich models simulated experimental data well but the PSO model simulated most, based on the correlation coefficient R^2 (> 0.95) values. The Boyd model confirmed that the adsorption process was controlled by liquid film diffusion and the effective diffusion coefficients were very low. The q_e values decreased with increase in C_o, increase in pH and increase in adsorbent dosage. However the removal of MY from aqueous solution was very low. Treatment of carbon with dilute HNO_3 had no favorable impact.

***Keywords*:** Activated carbon, adsorption, *G. aborea* bark, kinetic models, metanil yellow

1. INTRODUCTION

Industries involved in the production of dyes, textiles, pharmaceuticals, tannery, food, etc., use dyes to impart color to their products. The textile industry consumes the largest quantity of dyes (Akinola and Umar, 2015). Dyes contain carcinogenic substances which can cause serious harm to aquatic life and end users of dye-polluted water (Hassan and Salih, 2013).

MY is a synthetic azo dye applied on wool, nylon, silk, paper, ink, aluminum, detergent, wood, fur, cosmetics, and as biological stain. It is hazardous when ingested and slightly hazardous when inhaled or contacts the eyes (Isiuku, 2015). Toxicity data reveals that oral feeding or intra-peritoneal and intra-testicular administration of MY in animals produces testicular lesions, causing seminiferous tubules to suffer damage, reducing the rate of spermatogenesis. On oral consumption, it causes methaemoglobinaemia (Sachdeva et al., 1992) and cyanosis (Chandro and Nagaraja, 1987) in humans, while skin contact results into allergic dermatitis (Hausen, 1994). MY also has tumor-producing effects and can also create intestinal (Ramachandani et al., 1997) and enzymic (Das et al., 1997) disorders in the human body. It is not mutagenic but can alter the expression of genes (Gupta et al., 2003).

A wide range of methods for the removal of dyes from wastewaters in order to alleviate environmental pollution have been developed. They include filtration, adsorption, coagulation, advanced oxidation, and ozonation (Tong et al., 2016). Among these technologies, adsorption is the best due to its low initial cost, flexibility, simplicity of design, ease of operation and insensitivity to toxic pollutants (Wang et al., 2010). Adsorption is a surface phenomenon where a substance binds to the surface of another on an atomic or molecular scale (Isiuku et al., 2014).

Activated carbon is the most commonly used adsorbent and has proved to be an effective material for the removal of various pollutants from wastewater (Isiuku and Nwosu, 2017). This is due to the fact that activated carbon has large surface area, with its micro-porous structure resulting in high adsorption capacity (Olawale et al., 2015). Commercial activated carbons are costly. This is due to the use of non-renewable and relatively expensive starting materials such as coal, which is unjustified in pollution control applications (Isiuku et al., 2014). Nigeria grows *G. aborea* in many parts of the South and Middle belt. The wood is used mainly as timber. The aim of this research is to convert the bark to activated charcoal and investigate its efficiency in removing an azo dye from simulated wastewater. This will help take care of the huge *G. aborea* bark waste.

2. MATERIALS AND METHODS

2. 1. Adsorbate

The MY also called C.I. Acid Yellow 36 (Merck, Switzerland) used in this study, was bought at Onitsha, Anambra State, Nigeria and used directly without further treatment. The structure of MY is shown in Fig.1. The stock solution was prepared by dissolving 1g dye per liter solution using distilled water. Different solution concentrations (25 – 100 mg/L) used in this adsorption process were obtained by dilution of the stock solution. 0.1 M HNO_3 and 0.1M NaOH solutions were used for pH adjustments.

2. 2. Preparation of activated carbon

The dry *G. aborea* bark obtained from *G. aborea* trees at Owerri, Nigeria, was washed three times with distilled water and dried in the sun. The biomass was ground and soaked in 20% $^{w}/_{v}$ H_3PO_4 at a ratio of 3 acid: 1 biomass by mass for 24h. Excess acid was filtered off and the biomass spread on a lattice to dry. The dry biomass was carbonized at 450 – 500 °C for 7h. After cooling, the carbon was washed with hot distilled water until pH of the filtrate was about 6. The washed carbon was dried in a hot-air oven at 110 °C for 2h. After cooling, the carbon was soaked in 0.1 M HNO_3 for 4h. Excess acid was filtered off and the carbon washed to pH ~6 with distilled water. The washed carbon was dried in a hot-air oven at 110 °C for 2h. It was then cooled and sieved to get 0.42 – 0.841 mm particles, and stored in an air-tight plastic container.

2. 3. Characterization of the activated carbon

The bulk and dry densities of the carbon were determined by the method of Ekpete et al.,(2012); Pore volume, by the method of Mohammed et al., (2012); Porosity (Ekpete et al., 2012); Specific surface area by the ethylene glycol monoethyl ether (EGME) method (Cerator and Luteneger, 2002), Iodine number, by the Gimba and Musa, (2005) method; pH by the ASTM - D 3838 – 80 standard test method (ASTM, 1996); moisture, volatile matter, ash and fixed carbon contents by the methods of Rengaraj et al., (2002)]; AOAC (2010); Ekpete, (2010) and the Isiuku et al., (2015) methods respectively. The point of zero charge pH, pH_{pzc}, was determined by the solid addition method (Akinola and Umar, 2015). In this method, 40ml portions of 0.1M KNO_3 solution were introduced into eleven 100-ml conical flasks. The pH values of the solution in the flasks were adjusted to 2 – 12 with 1M HNO_3 and 1M NaOH solutions. 0.2g portions of NATPAAC were added into the flasks which were then put in a water-bath shaker and agitated at 125 rpm for 5h at 30 °C and atmospheric pressure. The pH values of the supernatants were measured. Values of ΔpH were plotted against initial pH values. The point the plot cuts the initial pH axis is the pH_{pzc}. $\Delta pH = pH_f - pH_i$, where pH_f and pH_i are final and initial pH values**.**

2. 4. Batch adsorption study

Batch adsorption investigations were carried out by shaking 25 ml portions of known C_o of MY solution with 0.01 g carbon portions in 50 ml flasks. The effect of solution initial pH on the adsorption of the dye solution by NATPAAC was studied by contacting 25 ml of 25mg/L dye solution with 0.02 g carbon portions in various flasks of varying pH values (2 – 9) at 30 °C. The initial solution pH was adjusted by drop-wise addition of 1 M HNO_3 or 1M NaOH and the pH measured with a pH meter (Ohaus ST 10) The flasks were stoppered and placed in a water-bath shaker shaking at 175 rpm. Samples were withdrawn at 60min intervals, filtered through glass wool bed and the filtrate analyzed with a spectrophotometer (Shimadzu UV-752, Japan) at 440 nm λ_{max}.

The quantities of MY adsorbed per unit mass of adsorbent at time t, q_t (mg/g) and at equilibrium q_e (mg/g) were determined using Eqs. 1 and 2:

$$q_t(mg/g) = \frac{(C_o - C_t)V}{1000x} \quad \ldots\ldots\ldots\ldots\ldots\ldots\ldots\ldots\ldots\ldots\ldots (1)$$

$$q_e(mg/g) = \frac{(C_o - C_e)V}{1000x} \quad \ldots\ldots\ldots\ldots\ldots\ldots\ldots\ldots\ldots\ldots\ldots (2)$$

where, C_t and C_e (mg/L) are the liquid-phase concentrations of the dye at time t, and at equilibrium respectively. V (cm^3) is the volume of the solution and x (g) the mass of dry adsorbent used.

3. RESULTS AND DISCUSSION

3. 1. Characterization of activated carbon

The physicochemical parameters of the adsorbent are shown in Table 1. Fig. 2 indicates the point of zero charge pH which is 3.4. This shows that above pH 3.4, adsorption of MY would be low. This is due to the fact that the surface of the carbon is negatively charged, hence repulsion of the MY ions which are also negatively charged (Akinola and Umar, 2015).

3. 2. Effects of initial dye concentration and contact time

25 ml portions of C_o (25 – 100 mg/L) of MY solution were contacted with portions of 0.01 g NATPAAC from *G. aborea* bark at 30°C, initial pH 3 and at shaker speed 175 rpm for 360 min. Fig.3 shows decrease in q_e with time, reaching equilibrium at 240 min for 25 and 50 mg/L. C_o 100 mg/L showed virtually no adsorption. This might be due to competition among the dye anions for available binding sites on the adsorbent (Ekpete et al., 2010; Mahvi et al., 2004). The q_e values were 2.35, 1.00 and 0.48 mg/g for 25, 50, and 100 mg/L C_o respectively.

3.3. Effect of initial solution pH

The efficiency of adsorption is dependent on the pH of the solution because variation in pH leads to variation in the degree of ionization and the surface properties of the adsorbent (Mas Haris and Sathasivam, 2009: Gupta et al., 2007). 0.02 g adsorbent portions were contacted with 25ml portions of 25mg/L C_o at pH values 2 – 9. Fig.4 shows decrease in qe (mg/g) with increase in pH. The optimum pH was 2. At low pH, the surface of the adsorbent is largely protonated. The H^+ ions provide an electrostatic attraction between the adsorbent surface and the anionic dye particles which brings about maximum adsorption. At higher pH, the degree of protonation of the adsorbent surface becomes less resulting in decrease in diffusion and adsorption as a result of electrostatic repulsion (Mas Haris and Sathasivam, 2009; Khattri and Singh, 2009; Baztias and Sidiras, 2007). In alkaline medium (pH 9), lowest adsorption occurred as a result of competition between excess ^-OH ions and the dye anions for adsorption sites (Mas Haris and Sathasivam, 2009). The experimental results showed low pH as favorable for the adsorption of MY on NATPAAC from *G. aborea* bark.

3.4. Effect of adsorbent dosage

Different masses of the adsorbent (0.01 – 0.32 g) were contacted with 25 ml portions of the dye solution at 175 rpm shaker speed, C_o 25mg/L, pH 3 and temperature 30 °C. From Fig 5, it can be observed that q_e (mg/g) decreased with increase in adsorbent dosage. The result is in trend with the studies of Tsai et al., (2008) and Pokordi and Kumar, (2006). The trend can be as a result of splitting effect of flux (concentration gradient) between adsorbate and

adsorbent with increasing adsorbent concentration leading to a decrease in the quantity of dye adsorbed per mass of adsorbent (Koumanova et al., 2002).

3. 5. Adsorption kinetic modeling

Isotherms are obtained under equilibrium conditions whereas in most adsorption processes the retention time is too short for equilibrium to be attained. Hence information must be obtained on the time dependence of adsorption processes by carrying out process-oriented kinetic studies (Ho et al., 1995). Time - dependent experimental data in this work were analyzed with the Pseudo-second order, Elovich, Intra-particle diffusion, Liquid film diffusion and Boyd models.

3. 5. 1. Pseudo- second order (PSO) kinetic model

One of the linearized forms of the pseudo-second order kinetic models (Ekpete et al., 2012) in common use is expressed as Eq. 3:

$$\frac{t}{q_t} = \frac{1}{h_o} + \frac{t}{q_o} \quad \ldots\ldots\ldots\ldots\ldots\ldots\ldots\ldots\ldots \quad (3)$$

where, q_t (mg/L) is the adsorption capacity at time t (min), q_o (mg/g) the predicted equilibrium adsorption capacity of the adsorbent, h_o(mg/g/min) the initial adsorption rate and t(min). h_o is expressed as Eq.4:

$$h_o = k_2 q_o^2 \quad \ldots\ldots\ldots\ldots\ldots\ldots\ldots\ldots\ldots\ldots (4)$$

where, k_2 (g/mg/min) is the second order rate constant. A plot of t/q_t against t yielded a straight line with slope $^1/q_o$ and intercept $^1/h_o$ (Fig. 6).

Table 1 shows the values of q_o, k_2 and R^2. The correlation coefficient R^2 values which are greater than 0.95 show that the PSO model is a very good fit for experimental data.

3. 5. 2. Elovich model

The linearized form of the Elovich model equation is expressed as Eq.5. It is valid for systems in which the adsorbing surface is heterogeneous (Mittal et al., 2008).

$$q_t = \frac{1}{\beta} In(\alpha\beta) + \frac{1}{\beta} Int \quad \ldots\ldots\ldots\ldots\ldots\ldots\ldots\ldots\ldots\ldots (5)$$

A plot of q_t against ln t gave a straight line with slope $^1/\beta$ and intercept ($^1/\beta$) ln (α β)
Where, α is the initial adsorption rate (mg/g min) and β (mg/g) is related to the extent of surface coverage and the activation energy for chemisorptions (Fig. 7). The values of α, β and R^2 are shown in Table 1. The R^2 values 0.9195, 0.9168 and 0.7656 for C_o 25, 50 and 100 mg/L respectively show this model good for analyzing experimental data.

3. 6. Adsorption mechanism

To interpret experimental data, it is necessary to recognize the adsorption process steps which govern the overall removal rate in each case (Crank, 1956)). During the adsorption of an adsorbate by a porous adsorbent, the adsorbate undergoes either particle diffusion or film diffusion or is adsorbed on the interior surface of the adsorbent. The third process is very fast and is not the rate-limiting step in the adsorption (Srivastava et al., 2006; Kannam and Sundaram, 2001).

The remaining two steps have three possibilities:

- If external transport is greater than internal transport, rate is governed by particle diffusion
- If external transport is less than internal transport, rate is governed by film diffusion
- If external transport and internal transport are nearly or are equal, there occurs the formation of a liquid film surrounded by the adsorbent particles, as the transport of the adsorbate ions to the boundary does not occur at a considerable rate

The intra-particle diffusion, liquid film diffusion and Boyd models were applied in this work to establish the process involved.

3. 6. 1. Intra-particle diffusion model

The possibility of intra-particle diffusion being the rate determining step in the adsorption process can be ascertained using the intra-particle diffusion model (Boyd et al., 1974). Involved in the process are the transport of the adsorbate to the surface of the adsorbent and the diffusion of the adsorbate particles into the interior of the pores of the adsorbent which is usually a slow process. Based on this theory,

$$q_t = k_{id} t^{0.5} + 1 \quad \ldots\ldots\ldots\ldots\ldots\ldots\ldots\ldots\ldots\ldots\ldots\ldots \quad (6)$$

where, K_{id} (mg/g/min$^{0.5}$) is the intra-particle diffusion rate constant and I is the constant that gives idea about the thickness of the boundary layer. The larger the value of I the greater is the boundary layer effect (Njoku and Hameed, 2011).

If a plot of q_t against $t^{0.5}$ gives a straight line, then the adsorption process is controlled by intra-particle diffusion only and the slope gives the rate constant, K_{id}. However, if the data show multi-layer plots, two or more steps controlled the adsorption process. Fig.8 shows analysis of experimental data with this model. Results show that the removal of MY by NATPAAC from *G. aborea* bark was not controlled by intra-particle diffusion.

3. 6. 2. Liquid-film diffusion model

When the liquid phase up to the solid phase boundary plays a major role in adsorption, then the liquid film diffusion model equation is used. The equation is expressed as Eq. 7:

$$In(1 - F) = -K_{id} t \quad \ldots\ldots\ldots\ldots\ldots\ldots\ldots\ldots\ldots\ldots\ldots\ldots \quad (7)$$

where, F (where $q_t < q_e$) is the fractional attainment of equilibrium expressed as Eq. (8)

$$F = {}^{q_t}/_{q_e} \ldots\ldots\ldots\ldots\ldots\ldots\ldots\ldots\ldots\ldots\ldots\ldots\ldots\ldots\ldots\ldots\ldots\ldots. \quad (8)$$

K_{id} (min^{-1}) is the adsorption rate constant and t the time (min). A linear plot of –ln (1 – F) against t giving a straight line with zero intercept, suggests that the adsorption process is controlled by diffusion through the liquid surrounding the adsorbent (Ekpete et al., 2012). Fig.9 shows modeling experimental data with the liquid film diffusion model. The figure shows that none of the lines (for C_o 25, 50 and 100 mg/L) passed through zero. Hence the adsorption was not solely controlled by liquid film diffusion.

3. 6. 3. Boyd model

In order to establish the actual mechanism involved in the adsorption of MY on NATPAAC from *G. aborea* bark, the Boyd kinetic model (Boyd et al., 1974; Njoku and Hameed, 2011; Reinchenberg, 1953) was applied. The Boyd model equation is expressed as Eq. 9:

$$F = 1 - \frac{6}{\pi^2}\sum_{n=1}^{\infty}\frac{1}{n^2}\,exp(-n^2B_t) \ldots\ldots\ldots\ldots\ldots\ldots\ldots..(9)$$

where, B_t is a mathematical function of F at time t. Eq. (7) can be simplified with approximations to give Eqs. 10 and 11

$$B_t \;=\; -0.4977 - In(1-F) \;\; for \;\; (F > 0.85) \;\ldots\ldots\ldots\ldots\ldots (10)$$

$$B_t \;= \left[\sqrt{\pi} - \sqrt{\pi - \left(\frac{\pi^2 F}{3}\right)}\right]^2 \; for\ (F \;\leq 0.85) \ldots\ldots\ldots\ldots\ldots\ldots\ldots\ldots\ldots..(11)$$

A plot of B_t against t gives a straight line which can be used to determine the rate-determining step in the adsorption process. A straight line which passes through the origin for a given C_o is the rate-determining step in the adsorption process. If the plot is nonlinear or linear but does not pass through the origin, then the adsorption process is controlled by liquid diffusion. Fig. 10 shows that the adsorption of MY on NATPAAC from *G. aborea* bark was controlled by liquid film diffusion for all the C_o values since none of the straight lines passed through the origin.

The slope of the B_t (Boyd time constant after time t) versus time t gives B, the time constant which can be used to determine the effective diffusion coefficient for any C_o. B is expressed as Eq. 12:

$$B = \frac{\pi^2 D_i}{r_o^2} \;\ldots\ldots\ldots\ldots\ldots\ldots\ldots\ldots\ldots\ldots\ldots\ldots\ldots\ldots\ldots\ldots\ldots\ldots.(26)$$

where, r is the radius of adsorbent particle. The average particle size of carbon used in this work was 3.532×10^{-3} m. Table 2 shows the B, D_i and R^2 values for C_o 25, 50 and 100 mg/L respectively. The Boyd time constant and the effective constant increased with increase in C_o.

4. CONCLUSIONS

NATPAAC was produced form *G. aborea* bark. The carbon was used to remove MY from aqueous solution by batch adsorption at 30 °C. The optimum time for the adsorption was 300 min. The optimum C_o, pH 2 and adsorbent dosage were 25 mg/L, 2 and 0.01 g/25 ml solution respectively. The optimum q_e was 2.35 mg/g. q_e was found to decrease with increase in C_o, increase in pH and increase in adsorbent dosage. The PSO and Elovich kinetic models simulated experimental results well though the PSO was a better fit based on R^2 values. The Boyd model was used to confirm liquid film diffusion as the rate-determining step. However, the adsorption of MY on NATPAAC from *G. aborea* bark was very low.

References

[1] Akinola, L. K. & Umar, A. M., (2015). Adsorption of crystal violet onto adsorbents derived from agricultural wastes: kinetic and equilibrium studies, *J. Appl. Sci. Environ. Manage*. 19 (2), 279-288

[2] Hassan, A. A. & Salih, Z. A., (2013). Methylene blue removal from aqueous solution by adsorption on eggshell bed. *Euphrates J. Agric. Sci*. 5 (2), 11-23

[3] Isiuku, B. O., (2015)., Adsorption of metanil yellow and methyl red from aqueous solution using cassava peels activated carbon in a fixed-bed column. *PhD dissertation*, University of Port Harcourt, Port Harcourt, Nigeria

[4] Sachdeva, S. M., Mani, K. V., Adval, S. K., Jolpota, V. P., Rasela, K. C. & Chadha, D. S., (1992). Acquired toxic methaemoglobinaemia. *J. Assoc. Physicians Ind*., 40, 239-240

[5] Chandro, S. S. & T. Nagaraja, T., (1987). A food-poisoning out-break with chemical dye: an investigation report. *Med. J. Armed Forces Ind*., 43, 293-300

[6] Hausen, B. M., (1994). A case of allergic contact dermatitis due to metanil yellow. *Contact Dermatits*, 31, 117-118

[7] Ramachandani, S, Das, M., Joshi, A. & Khanna, S. K., (1997). Effect of oral and parental administration of metanil yellow on some hepatic and intestinal biochemical parameters. *J. Appl. Toxicol*. 17, 85-91

[8] Das, M., Ramachandani, S., Upreti, R. K. & Khanna, S. K., (1997). Metanil yellow: a bifunctional inducer of hepatic phase I and phase II xenoblastic-metabolizing enzymes. Food *Chem. Toxicol*. 35, 835-838

[9] Gupta, S., Sundarrajan, M. & Rao, K. V. K., (2003). Tumour promotion by metanil yellow and malachite green during rat hepatocarcinogenesis associated with dysregulated expression of cell cycle regulatory proteins. *Tetragon Carcin. Mut*. (Suppl. I), 301-312

[10] Tong, Z., Zheng, P., Bai, B., Wang, H. & Y. Suo, Y., (2016). Adsorption performance of methyl violet via α – Fe_2O_3 @ porous hollow carbonaceous microspheres and its

effective regeneration through a Fenton – like reaction. *Catalysts*, 6, 58: doi: 10.3390/catal6040058

[11] Wang, L., Zhang, J., Zhao, R., Li, C., Li, Y & Zhang, C., (2010). Adsorption of basic dyes on activated carbon prepared from *Polygnum orientale* Linn: Equilibrium, kinetic and thermodynamic studies. *Desalination*, 254, 68-74

[12] 12. Isiuku, B. O., Horsfall Jnr., M, & Spiff, A. I., (2014). Colour removal from a simulated methyl red wastewater by adsorption on carbon in a fixed bed. *Res. J. Appl. Sci*. 9 (4), 201-207

[13] Isiuku, B. O. & Nwosu, C. N., (2017). Fixed-bed adsorption of metanil yellow from aqueous solution on HNO_3-treated-H_3PO_4-activated carbon frm gmelina bark. *Asian J. Chem*. 29 (3), 475-479

[14] Olawale, A. S., Ajayi, O. A., Olakunle, M. S., Ityokumbul, M. T. & Adefila, S. S., (2015). Preparation of phosphoric acid activated carbons from *Canarium schweinfurthii* nutshell and its role in methylene blue adsorption. *J. Chem. Eng. Mater. Sci*. 6 (2), 9-14

[15] Ekpete, O. A., (2012). Adsorption and kinetic studies of phenol and 2-chlorophenol onto fluted pumpkin (*Telfairia occidentalis*, Hook) stem waste activated carbon. *PhD Dissertation*, University of Port Harcourt, Port Harcourt, Nigeria

[16] Mohammed, A., Aboje, A. A., Auta, M. & Jibril, M., (2012). Comparative analysis and characterization of animal bones as adsorbent. *Adv. Appl. Sci. Res*. 3 (5), 3089-3096

[17] Cerator, A. B. & Luteneger, A. J,. (2002). Determination of surface area of fine grained soils by the ethylene glycol monoethyl ether (EGME) method. *J. Geotechnol. Testing*, 25 (3), 1-7

[18] Gimba, C.& Musa, I., (2005). Adsorption of phenol and some toxic metals from textile effluent. In: *Proceedings of the 28th annual International Conference of Chemical Society of Nigeria*, 32, 167-170

[19] American Society for Testing and Materials, (1996). *Annual Book of ASTM Standard* 15.01 Refractories, Carbon and Graphic Products; Activated Carbon, ASTM, Philadelphia PA

[20] Rengaraj, S., Seung-Hyeon, M. & Sivabam, S., (2002). Agricultural solid waste for the removal of organics: adsorption of phenol from water and wastewater by palm seed coat activated carbon. *Waste Manage*. 22, 534-548

[21] Association of Official Analytical Chemists. (2010). www.aoac.org/ISPAM/pdf/3.5%20SMPR%20Guideline%20v12.1.pdf (2019) assessed on 13th February, 2012

[22] Ekepete, A. O., Horsfall Jnr., M. & Spiff, A. I., (2010). Removal of chlorophenol from aqueous solution using fluted pumpkin and commercial activated carbon. *Asian J. Nat. Appl. Sci*. 14, 321-326

[23] Mahvi, A., Maleki, A. & Eslami, A., (2004). Potential of rice husk and rice husk ash for phenol removal in aqueous systems. *Amer. J. Appl. Sci*. 14, 321-326

[24] Mas Haris, M. R. H. & Sathasivam, K., (2009). The removal of methyl red from aqueous solution using banana pseudo-stem fibres. *Amer. J. Appl. Sci*. 6 (9), 1690-1700

[25] Gupta, V. K., Jain, R., Varshney, R. & Saini, V. K., (2007). Removal of Reactofix Navy Blue 2 GFN from aqueous solution using adsorption techniques. *J. Colloid Interf. Sci*. 307, 326-332

[26] Khattri, S. D. & Singh, M. K., (2009). Removal of malachite green from dye wastewater using neem sawdust by adsorption. *J. Hazard. Mater*., doi: 10.1016/j:jhazmat.2009.01.101

[27] Baztias, F. A. & Sidiras, D. K., 2007. Dye adsorption by prehydrolysed beech sawdust in batch and fixed-bed systems. *Bioresour. Technol*. 98, 1208-1217

[28] Tsai, W-T., Hsien, K-J., Hsu, H-C., Lin, C-M., Lin, K-Y. & Chiu, C-H., (2008). Utilization of ground eggshell waste as an adsorbent for the removal of dyes from aqueous solution. *Bioresour. Technol*., 99, 1623-1629

[29] 29. Pokordi, K. & Vasanth Kumar, K., (2006). Equilibrium, kinetics and mechanism modeling and simulation of basic and acid dyes sorption onto jute fiber carbon: Eosine yellow, malachite green and crystal violet single component systems. *J. Hazard. Mater*. (2006), doi:10.1016/jhazamt.2006.09.029

[30] Koumanova, B., Peeva, P., Allen, S. J., Gallagher, K. A. & Healy, M. G., (2002). Biosorption from aqueous solutions by eggshell membrane and *Rhizopus oryzae*: Equilibrium and Kinetic studies. *J. Chem. Technol. Biotechnol*. 77, 539-545

[31] Ho, Y. S., John, W. D. & Foster, C. F., (1995). Batch nickel removal from aqueous solution by Sphanum moss peat. *Water Res.* 29, 1327-1332

[32] Ekpete, O. A., Horsfall Jnr., M. & Spiff, A. I., (2012). Kinetics of chlorophenol adsorption onto commercial fluted pumpkin activated carbon in aqueous systems. *Asian J. Nat. Appl. Sci*. 1(1), 106-117

[33] Mittal, A., Gupta, V. K., Malviya, A. & Mittal, J., (2008). Process development for the batch and bulk removal and recovery of a hazardous water-soluble azo dye (Metanil Yellow) by adsorption over waste materials (Bottom Ash and De-oiled Soya). *J. Hazard. Mater*. 151, 821-832

[34] Crank, J., The Mathematics of Diffusion. Clarenden Press, Oxford, (1956)

[35] Srivastava, V. C., Swammy, M. M., Hall, I. D., Prasad, B. & Mishra, I. M., (2006). Adsorptive removal of .phenol by bagasse fly ash and activated carbon: Equilibrium, kinetics and thermodynamics. *Colloid Surf. A. Physicochem. Eng. Aspects*, 272, 89-104

[36] Kannam, N. & Sundaram, S., (2001). Kinetics and mechanism of removal of methylene blue by adsorption on various carbons: Comparative study. *Dyes and Pigments*, 51, 25 - 40

[37] Boyd, G. E., Adamson, A. W. & Myers, L. S., (1974). The exchange adsorption of ions from aqueous solutions by organic zeolites : II. Kinetics. *Amer. Chem. Soc*. 69, 2836-2848

[38] Njoku, V. O. & Hameed, B. H., (2011). Preparation and characterization of activated carbon from corn cob by chemical activation with H_3PO_4 for 2,4-dichlorophenoxyacetic acid adsorption. *Chem. Eng. J*. 173, 391-399

[39] Reinchenberg, D., (1953). Properties of ion exchangers resins in relations to their structures, III: Kinetics of exchange. *J. Amer. Chem. Soc*. 75, 589-597

(Received 30 July 2017; accepted 18 August 2017)

Table 1. Physicochemical characteristics of NATPAAC carbon from *G. aborea* bark

Parameters	**Values**
pH	5.8
Bulk Density (g/cm^3)	0.4
Porosity	0.82
Pore Volume (cm^3/g)	0.023
Specific Surface area (m^2/g)	350.41
Iodine number (mg/g)	53.49
Moisture content (%)	8.7
Volatile matter content (%)	45.4
Fixed carbon content (%)	36.37
Ash content (%)	9.53
pH_{pzc}	3.4

Table 2. Kinetic model parameters for the batch adsorption of MY on NATPAAC from *G. aborea* bark

Model/Parameter	Value		
	C_o (mg/L)		
	25	50	100
PSO			
q_o (mg/g)	1.914	0.804	0.447
q_e (mg/g)	2.35	1.000	0.48
k_2 (h^{-1})	0.974	0.9529	0.1053
R^2	0.974	0.9529	0.9951
ARE	0.186	0.196	0.069
Elovich			
β (g/mg)	0.2294	0.2092	9.7943
α (mg/gh)	2368	1699.35	315464.05
R^2	0.9195	0.9168	0.7656
Liq. film diff.			
K_{ld} (h^{-1})	0.4523	0.6191	0.7155
R^2	0.8608	0.7418	0.75

Boyd			
B	0.268	0.354	0.474
D x 10^{-7} (m^2/h)	3.388	4.475	5.991
R^2	0.8608	0.7418	0.75

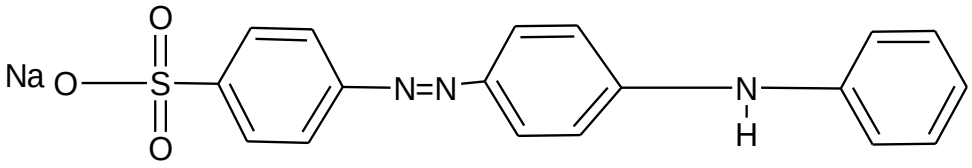

Fig. 1. Structure of metanil yellow

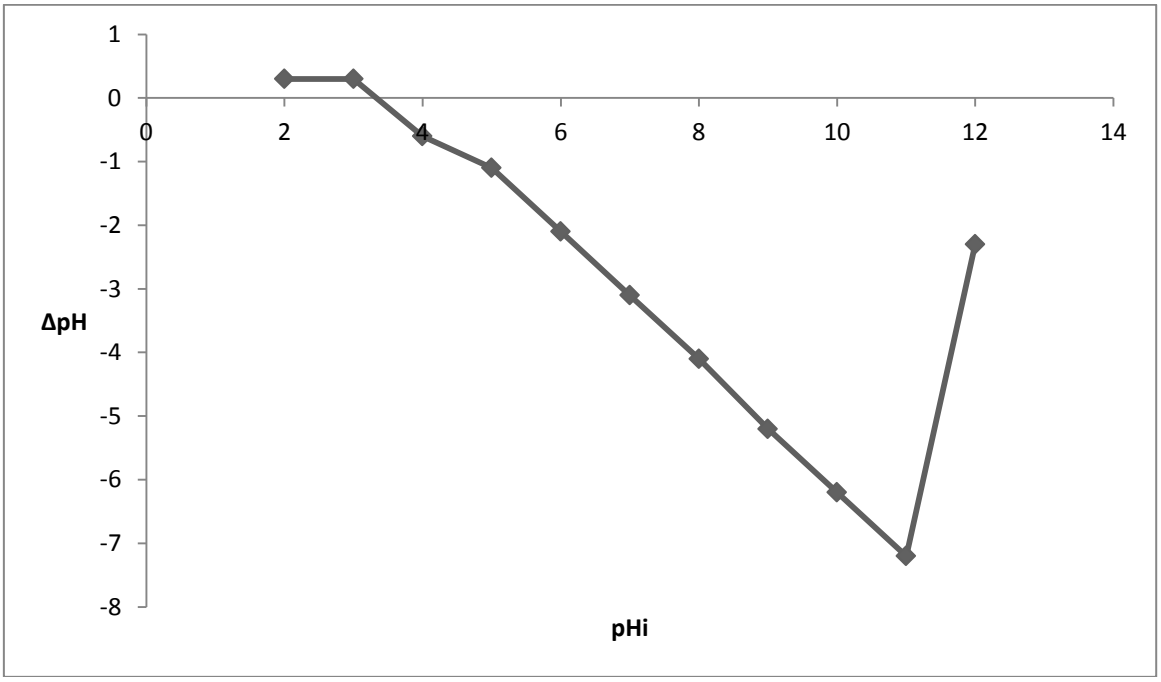

Fig. 2. Plot to determine point of zero charge pH of NATPAAC from *G. aborea*

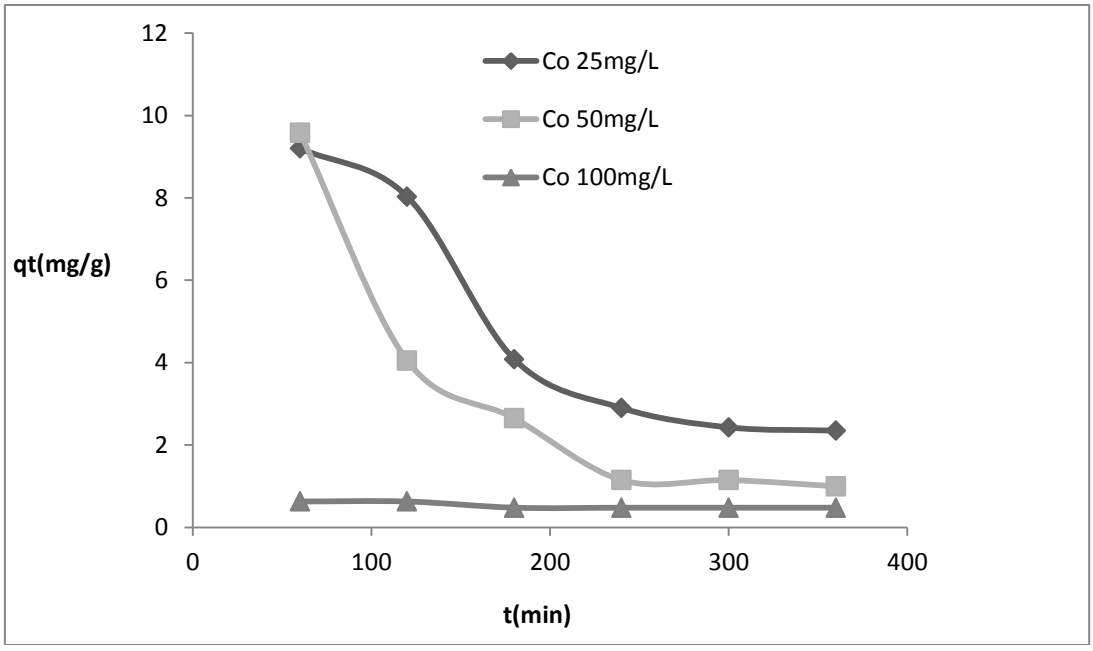

Fig. 3. Adsorption of MY on NATPAAC from *G. aborea* bark at various C_o values

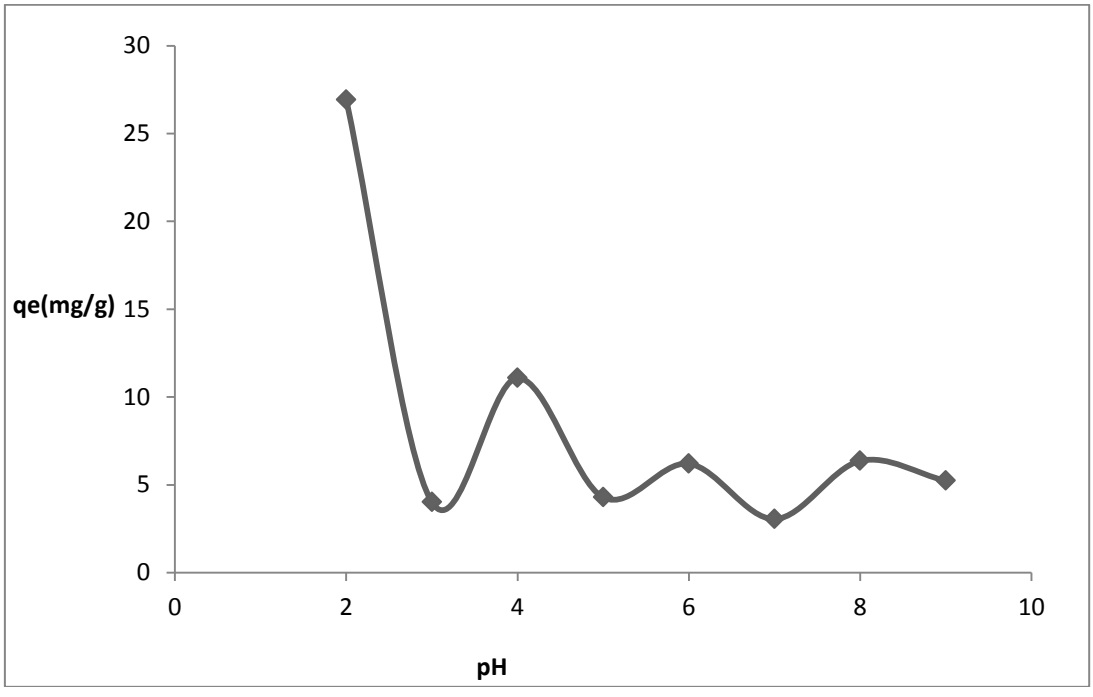

Fig. 4. Adsorption of MY on NATPAAC from *G. aborea* bark at various pH values

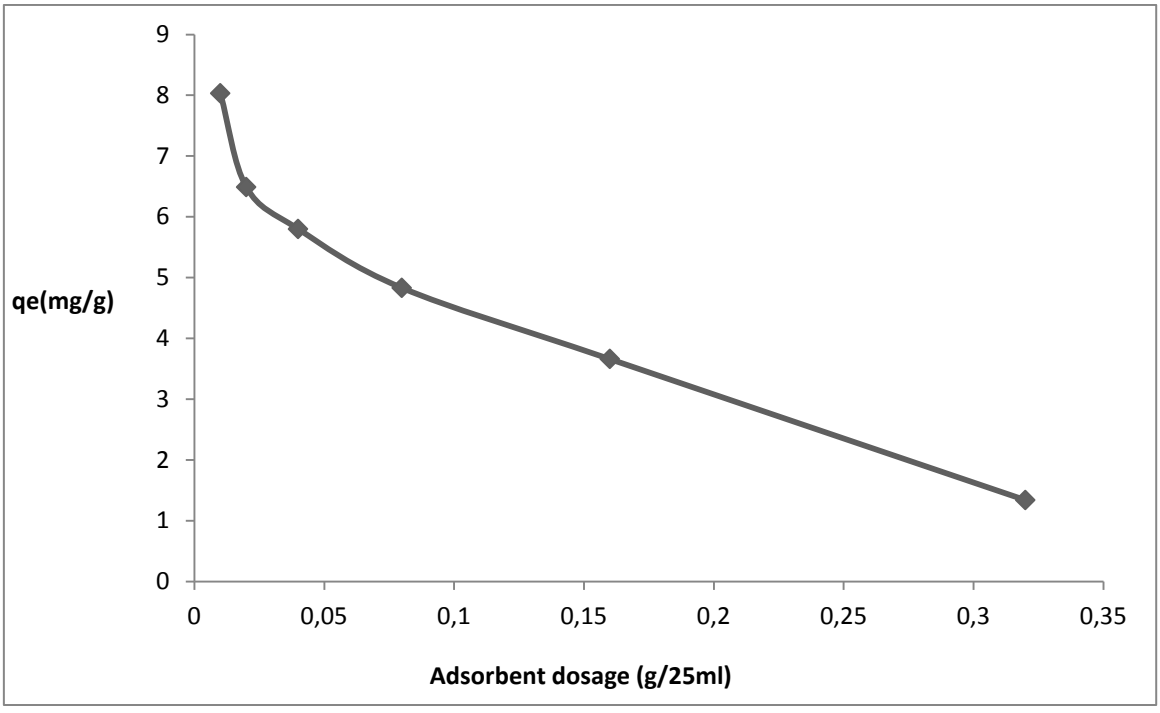

Fig. 5. Adsorption of MY on NATPAAC from *G. aborea* bark at various adsorbent dosages

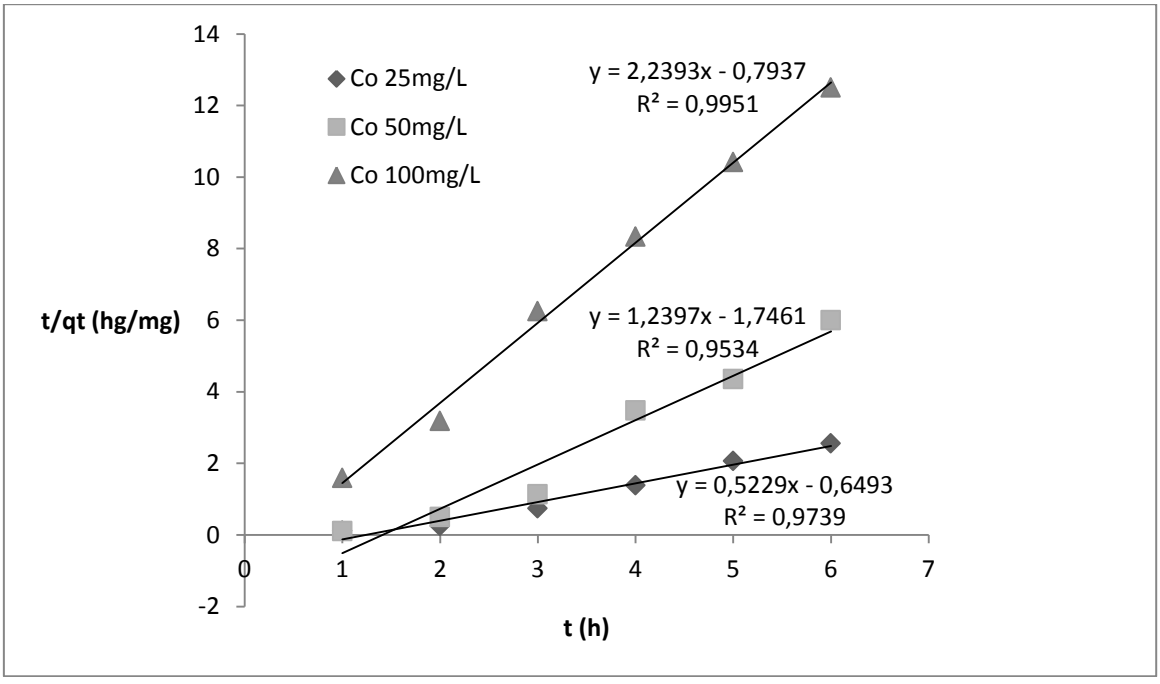

Fig. 6. Pseudosecond –order kinetic model plots for the adsorption of MY on NATPAAC from *G. aborea* bark at various C_o values

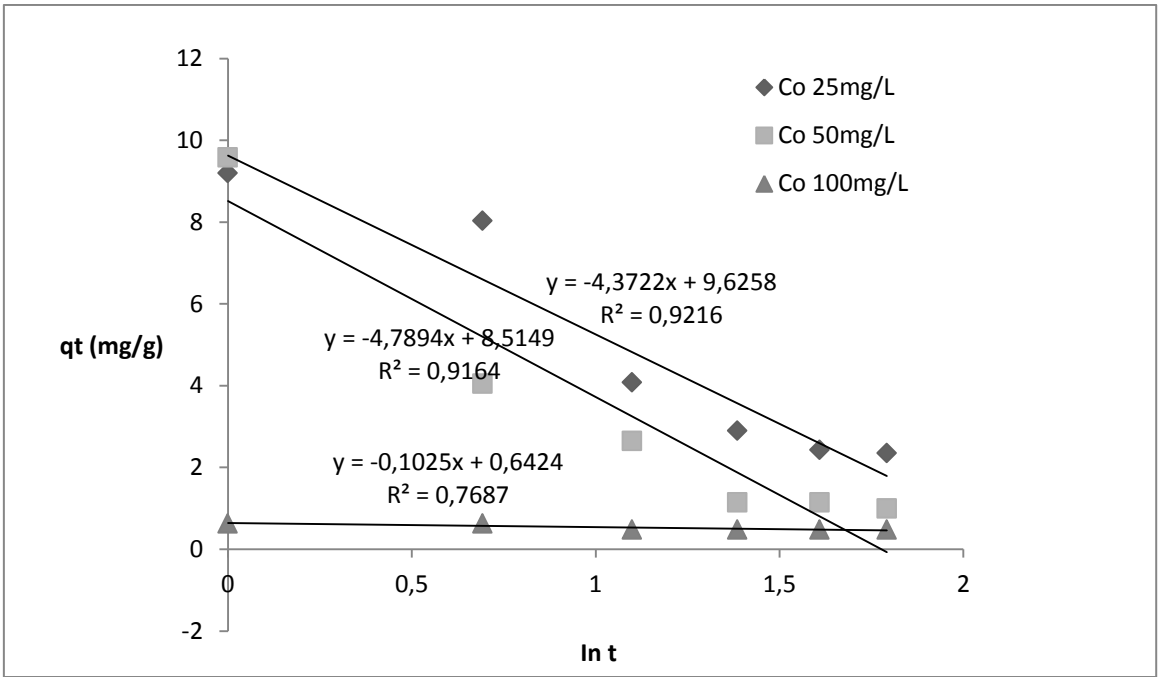

Fig. 7. Elovich model plot for the adsorption of MY on NATPAAC from *G. aborea* bark at various C_o values

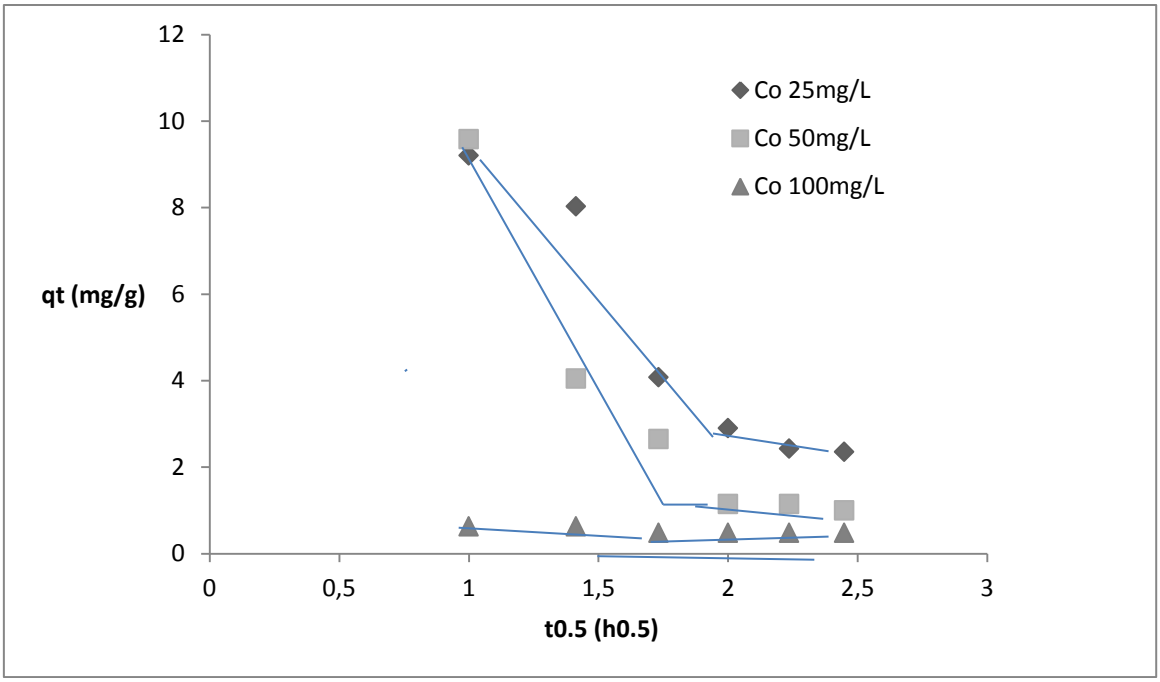

Fig. 8. Intra-particle diffusion model plots for the adsorption of MY on NATPAAC from *G. aborea* bark at various C_o values

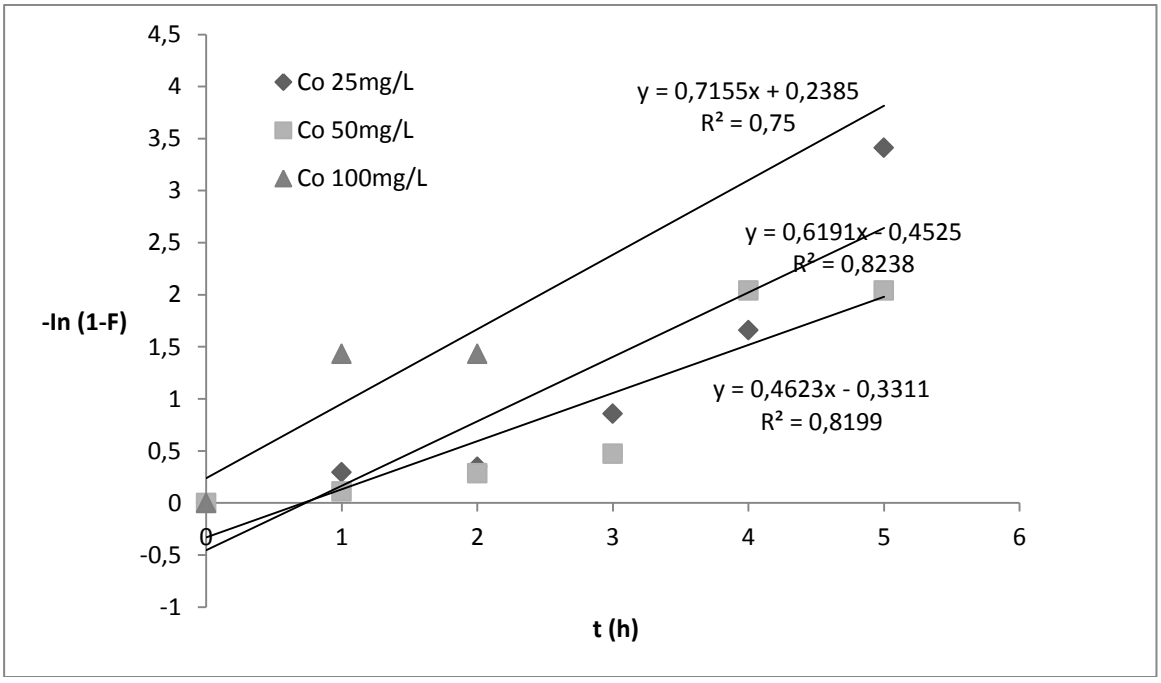

Fig. 9. Liquid Film diffusion model plots for the adsorption of MY on NATPAAC from *G. aborea* bark at various C_o values

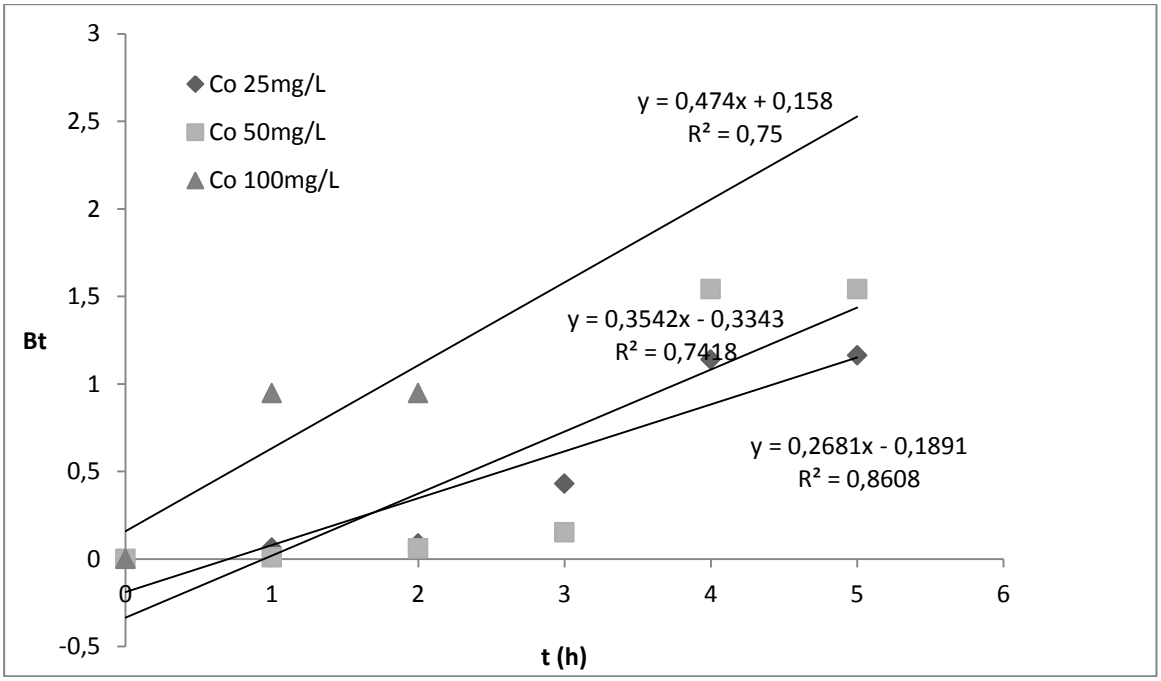

Fig. 10. Boyd model plots for the adsorption of MY on NATPAAC from *G. aborea* at various C_o values at 29 °C